Applied Energy 283 (2021) 116270

Contents lists available at ScienceDirect

Applied Energy

journal homepage: www.elsevier.com/locate/apenergy

Temperature optimization for improving polymer electrolyte membrane-water electrolysis system efficiency

Fabian Scheepers [a,*], Markus Stähler [a], Andrea Stähler [a], Edward Rauls [a], Martin Müller [a], Marcelo Carmo [a], Werner Lehnert [a,b]

[a] Forschungszentrum Juelich GmbH, Institute of Energy and Climate Research, IEK-14: Electrochemical Process Engineering, 52425 Juelich, Germany
[b] RWTH Aachen University, Germany

HIGHLIGHTS

- Modelling the overall system efficiency of PEM water electrolyzers.
- PEM water electrolysis efficiency can be significantly improved by temperature optimization.
- Optimal temperature depends on the applied cell voltage.
- Safety issue caused by hydrogen crossover is prevented by temperature optimization.

ARTICLE INFO

Keywords:
PEM electrolyzer
Temperature optimization
Efficiency optimization
Modeling

ABSTRACT

Most of the hydrogen produced today is made using fossil fuels, making a significant contribution to global CO_2 emissions. Although polymer electrolyte membrane water-electrolyzers can produce green hydrogen by means of excess electricity generated from renewable energy sources, their operation is still not economical. According to industry experts, the necessary cost reductions can be achieved by 2030 if system efficiency can be improved. The commonly stated idea is to improve efficiency by increasing the stack temperature, which requires the development of more resistant materials. This study investigates not only the efficiency of an electrolysis cell, but of the entire electrolysis process, including gas compression of hydrogen. The results indicate that an optimal stack temperature exists for every operating point. It is shown that the optimal temperature depends solely on the electrode pressure and cell voltage and can be analytically calculated. In addition, the temperature optimization leads to significantly reduced hydrogen permeation at low current densities. In combination with the pressure optimization, the challenging safety issues of pressurized electrolysis can be eliminated for the entire load range and, at the same time, the efficiency of the overall system be maximized.

1. Introduction

Hydrogen is an important feedstock in industrial chemical processes and is used in particular for the synthesis of ammonia-based fertilizers [1]. Today, 98% of industrial hydrogen production is based on fossil fuel processing, releasing more than 10 kg of CO_2 to produce 1 kg of H_2 [2]. With an annual production capacity of 70 million tons, [3] hydrogen production is therefore responsible for more than 2% of global CO_2 emissions. At the same time, much electricity is lost due to excess production from the fluctuating electricity supply of renewable energy technologies and the lack of viable storage systems [4]. Therefore, the production of green hydrogen as a chemical energy storage medium and feedstock for industrial processes has much to recommend it [5]. Splitting water in electrolyzers to produce hydrogen and oxygen is an option for achieving this goal [6]. However, this route is considerably more expensive than producing hydrogen with fossil fuels, [7] which is why it is important to improve efficiency and thus reduce costs [8].

Water electrolyzers can be divided into three technical categories: alkaline electrolysis (AE), polymer electrolyte membrane (PEM) electrolysis and solid oxide electrolysis (SOE). In 2017, experts forecast that PEM technology would be dominant by 2030, but critical gaps must still be closed [9]. These gaps are in the areas of materials, operating conditions, durability and economic viability [10]. It is obvious that the

* Corresponding author.
E-mail address: f.scheepers@fz-juelich.de (F. Scheepers).

https://doi.org/10.1016/j.apenergy.2020.116270
Received 22 June 2020; Received in revised form 11 November 2020; Accepted 13 November 2020
Available online 1 December 2020

Nomenclature

Parameter	Symbol
Faraday constant	F
Gibbs free energy	G
Enthalpy	H
Higher heating value	HHV
Lower heating value	LHV
Pressure	p
Entropy	S
Temperature	T
Cell voltage	U_{cell}
Voltage equivalency (LHV)	U_{LHV}
Voltage equivalency (vapor load)	U_{load}
Thermoneutral cell voltage	U_{th}
Heat of vaporization	$\Delta H^{vap}_{H_2O}$
Effort for external gas compression	$\eta^{c}_{H_2}$
Faraday efficiency	$\eta^{F}_{H_2}$
(Hydrogen) production efficiency	η^{p}
Overall system efficiency	$\eta^{tot}_{H_2}$

areas interact, for example, in that durability correlates with the operating conditions and materials used. Therefore, it is not surprising that many studies, investigating degradation, have come to the conclusion that durability declines with increasing stack temperature. It is reported that the ionic exchange resin is unstable when the temperature is increased above 80 °C [11]. This occurs due to chemical degradation, [12] which is more affected by temperature than by the current density [13]. This chemical degradation leads to membrane thinning, which should in fact reduce the cell resistance; however, an accelerated passivation of the titanium components overcompensates this effect [14]. In addition to the membrane, the dissolution rate of catalyst particles is also known to be increased at higher operating temperatures [15]. However, these arguments are countered by the fact that other studies indicate that efficiency increases with increasing stack temperature [16]. The stack temperature is reported to be the most dominant parameter affecting stack performance [17]. The reversible cell voltage declines with temperature [18] and the ionic conductivity of the membrane is improved [19]. From an electrochemical point of view, the electrocatalytic activity is enhanced when the temperature is increased, [20] which leads to faster reactions and less overpotential [21]. Additionally, a high temperature positively affects the system efficiency when the current density exceeds the value at which the efficiency is highest [22].

For the stated reasons, operating an electrolyzer always entails a compromise between efficiency and durability, but a closer look at this issue is merited. In the past, different electrolyzer models were developed to evaluate system performance. These have in common the fact that the overall efficiency of an electrolyzer is most significantly affected by its cell voltage efficiency. The polarization curve describes the voltage that must be applied to an electrolysis cell in order to generate a specific current between the electrodes of the cell. This is relevant, as the current is directly proportional to the amount of hydrogen produced and the cell voltage can be easily converted into the cell's voltage efficiency. Specifically, these studies dealt with various goals, such as optimizing the pressure mode with respect to the Faraday efficiency and compression work required to pressurize the produced hydrogen to storage pressure [23,24]. It was reported that the energetically-optimal pressure depends on the current density at which the system is operated and on the desired hydrogen storage pressure [25]. In addition, it was discussed whether the compression should be performed electrochemically within the stack or by external gas compressors [26]. In this regard, electrochemical compression appears to be beneficial, whereas differential pressure is preferable over balance pressure [27]. The modeling of high pressure applications, including experimental validation, was performed for systems that operate at more than 15 MPa [28]. It was also shown that besides the pressure, the temperature is of great importance [29]. However, thermal aspects are only rarely discussed [30]. Consequently, other temperature-dependent processes must be considered in more depth when modeling and operating an electrolysis system. In addition to the improvements in electrocatalytic activity and membrane conductivity with increasing temperature, gas permeation across the thin membrane and heat losses due to product gas saturation with water in the electrodes increases as well. The high significance of heat losses has already been shown when optimizing the efficiency of an electrolysis system by means of a pressure-optimized operating mode at constant stack temperature [31]. Herein, it is presented for the first time how the overall efficiency of an electrolysis system depends on the stack temperature, taking into account the effects mentioned above. This approach helps close the existing gaps mentioned and provides a new understanding of the impact of temperature on system efficiency.

2. Methodology

Electrolyzers efficiently produce hydrogen by splitting water with an electrical current. The hydrogen production efficiency, $\eta^{p}_{H_2}$, expresses the ratio of how much chemical energy is obtained and how much energy must be supplied to the electrolysis cell for this. The chemical energy obtained per mol of hydrogen is described by the lower heating value, which is 241.8 kJ per mol. If this value is divided by two times the Faraday constant, F, a cell voltage of 1.253 V alternatively results. On the other hand, the input energy can be separated into two parts: heat and electricity. The electrochemical splitting of liquid water requires a reversible cell voltage of 1.229 V and 48.6 kJ per mol of heat under standard conditions, which corresponds to an additional electrode potential of 0.252 V. These add up to the so-called thermoneutral cell voltage, U_{th}, which is 1.481 V. At cell voltages below this value, heat from ambient must be consumed, while excess heat is generated above this value. Therefore, the net heat flow is zero at 1.481 V. Ultimately; the maximum thermodynamic efficiency should be about 84.6% :

$$\eta^{p}_{H_2,max} = \frac{\frac{H_{LHV}}{2F}}{\frac{\Delta G_{HHV}}{2F} + \frac{T\Delta S_{HHV}}{2F}} = \underbrace{\frac{1.253V}{1.229V + 0.252V}}_{=U_{th}} \approx 84.6\% \quad (1)$$

In addition to this view, there is another aspect to be considered for continuously operating electrolyzers that affects the input energy required, namely that during operation, hydrogen and oxygen are produced and loaded with steam before being released from the system. However, this process requires additional enthalpy, which depends on the heat of vaporization, $\Delta H^{vap}_{H_2O}$, and the partial pressures, $p^{cat}_{H_2}$ and $p^{an}_{O_2}$, in the electrodes. Analogously to what is outlined above, this enthalpy can be converted into a voltage that is termed U_{load} in this work. Adding this voltage to the denominator of Eq. (1) results in the actual cell voltage at which no external heat must be supplied. It also determines the actual maximum efficiency of hydrogen production when operating an electrolyzer (derivation in the Appendix):[31]

$$\eta^{p}_{H_2,max} = \frac{1.253V}{U_{th} + U_{load}} = \frac{1.253V}{1.229V + 0.252V + p_{H_2O} \cdot \left(\frac{1}{p^{cat}_{H_2}} + \frac{1}{2p^{an}_{O_2}}\right) \cdot \frac{\Delta H^{vap}_{H_2O}}{2F}} \quad (2)$$

With regard to the application of PEM water electrolyzer, the anode is typically operated at low pressure, thus making the concerning term relevant. In contrast, the cathode term can be negligible for operation at elevated pressure.

While 1.229 V is, in theory, sufficiently high to produce hydrogen under standard conditions, in order to improve the reaction rates and charge transfer through the electrolysis cell, the cell voltage that must be applied is higher than this value. The resulting increase in current is

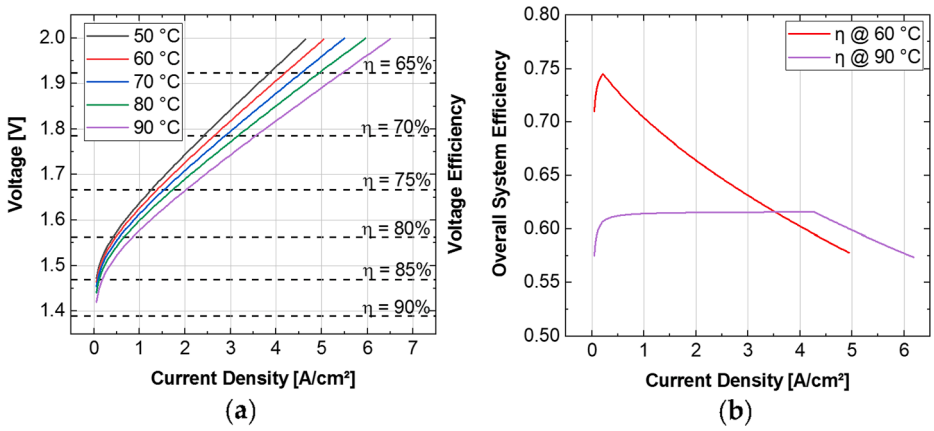

Fig. 1. **(a)** Plot of the cell voltage as a function of current density at different stack temperatures. The dashed lines symbolize the voltage efficiency according to Eq. (3); **(b)** plot of the overall efficiency of the system as a function of current density at stack temperatures of 60 °C and 90 °C. The cathode pressure is set to 0.2 MPa, while the anode is at ambient pressure.

directly proportional to the hydrogen production rate. At the same time, the additional voltage drop along the cell causes Joule heating, by which the need for external heating decreases. If the cell voltage, U_{cell}, applied is lower than the denominator of Eq. (2), external heating is still required and the efficiency of hydrogen production is correctly described according to the equation above. Otherwise, the cell must be cooled if the voltage is higher than the denominator of Eq. (2), as Joule heating generates more heat than required. Accordingly, the hydrogen production efficiency is worse than that described by Eq. (2). While cooling is performed by increasing the circulation rate of water through the system, the energy effort can be assumed to be negligible [25]. Therefore, the efficiency of hydrogen production approaches the so-called voltage efficiency with sufficient precision:

$$\eta^{p}_{H_2,volt} \approx \frac{U_{LHV}}{U_{cell}} = \frac{1.253\text{V}}{U_{cell}} \tag{3}$$

The cell voltage is the sum of the reversible cell voltage and the overpotential of the cell. The overpotential is mainly influenced by the catalyst activation and ion transport resistance in the membrane. For each of these contributions, the cell voltage decreases when the stack temperature is increased or, inversely, more hydrogen is produced at the same cell voltage (equations in the Appendix). This leads to the above-cited statements that the efficiency of the electrolyzer is improved by increasing the stack temperature. Typical cell voltages for operating PEM electrolyzers are between 1.6 V and 2.0 V, [32] while a temperature of up to 90 °C is desirable to maximize the efficiency [10]. Interviews with experts on water electrolysis have revealed that by 2030, electrolyzers should achieve an efficiency between 70% [33] and 71% [34], excluding external compression, purification and hydrogen storage. Eq. (3) can be used to calculate the associated cell voltage of 1.76 V to achieve this goal. Values of between 1.7 V [35] and 1.8 V [15] as the reference cell voltage are also recommended by other experts and institutions.

In real electrolysis systems, the amount of hydrogen produced differs from the amount of hydrogen that can actually be stored. The ratio of the actual value to the apparent value is called the Faraday efficiency, $\eta^{F}_{H_2}$. The predominant type of hydrogen loss is permeation through the membrane to the anode-side with recombination and thus elimination of the hydrogen and oxygen generated. The permeability increases with increasing gas pressure in the electrode and decreasing membrane thickness, but also with increasing stack temperature (equations in the Appendix) [36].

In addition to the production of storable hydrogen, there is a further loss of efficiency due to peripheral processes and devices outside the system. It has been demonstrated that losses due to system components such as pumps are negligible compared to the energy required to operate an electrolysis stack [25]. It has also been shown that even gas drying is not energy-relevant for system efficiency if the cathode pressure is above 0.2 MPa [25]. Regarding the energy requirement, the most relevant process at the system level is compression of the gas produced. These must be included in the model, as an increase in gas pressure in the electrodes can reduce the total energy required, although the Faraday efficiency is reduced. For this reason, the efficiency of the system components is approximated by the effort to compress the gas, $\eta^{c}_{H_2}$, which is independent of the stack temperature (equations in the Appendix).

In total, the overall efficiency of the system, $\eta^{tot}_{H_2}$, depends on the efficiency of the hydrogen production process, the Faraday efficiency and the effort to externally compress the gas:

$$\eta^{tot}_{H_2} = \eta^{p}_{H_2}\eta^{F}_{H_2}\eta^{c}_{H_2} \tag{4}$$

In the following, this approach is used to evaluate the maximum overall efficiency of a system based on a Nafion 212 membrane with a thickness of 51 μm. More information on modelling the Faraday efficiency and gas compression efficiency as well as the parameter used for the simulations can be found in the Appendix, while a detailed description of this model is available in the literature [31].

3. Results and discussion

As mentioned in the introduction, it is commonly accepted that increasing the stack temperature results in better cell performance, which is due to improved electrochemical activity and better conductivity of the membrane. The results of this study are in clear agreement with this, as can be seen in Fig. 1a. The cell voltage that is required to achieve the same current density declines when the stack temperature increases at a constant cathode pressure of 0.2 MPa. While this result clearly indicates that the voltage efficiency increases with increasing stack temperature, the picture changes when the overall efficiency of the system is calculated. With a moderate current density, the overall efficiency of the system at a stack temperature of 60 °C is higher than that of the system with a stack temperature of 90 °C (see Fig. 1b). However, this state reverses at current densities above 3.5 A per cm^2, so that the cell with the higher voltage efficiency (compared with Fig. 1a) also achieves higher overall efficiency. At 3.5 A per cm^2, the cell voltage of the 90 °C system is at 1.80 V which is equal to an efficiency of 69%. But, if the goal of 71% system efficiency is to be achieved before gas compressing, purification and storage of the gas are achieved, the system must not be operated above a terminal cell voltage of 1.76 V if no Faraday losses are assumed. This surprisingly means that the cooler system performs more efficient.

However, it is usually proposed to operate a PEM-electrolyzer at

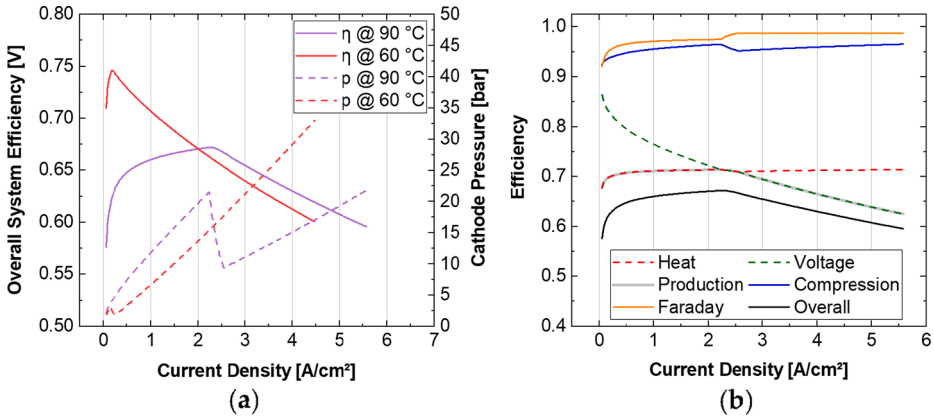

Fig. 2. **(a)** Plot of the optimized overall system efficiency and corresponding cathode pressure as a function of current density at different stack temperatures; **(b)** plot of the efficiency contributions as a function of current density at a stack temperature of 90 °C. The production efficiency is always the minimum of the heat-limited production efficiency and voltage efficiency.

elevated pressure. It is, therefore, interesting to witness what happens when an electrolyzer works under differential pressures when the anode is at ambient pressure. This can be achieved by evaluating the maximum overall system efficiency in terms of cathode pressure optimization. This approach has already been proposed in previous studies [25,31]. Three findings are obtained through this procedure (see Fig. 2a):

(a) It was observed that the terminal cell voltage is achieved at a lower current density, which clarifies the challenges when the goals for electrolysis cells are formulated that exclude peripheral process steps such as gas compression. The energy required for the compression is partly taken over by electrochemical compression in the cell, which increases the cell voltage according to the Nernst equation and makes the electrolysis cell less efficient. The efficiency of the overall system with compressors, however, improves. Therefore, the goal is redefined in this study so that the overall system efficiency is about 65% which includes a hydrogen compression to 20 MPa. This corresponds to an overall efficiency of 71% without taking the compressor into account for the stack operated at ambient pressure (see Fig. 1b). Consequently, the terminal cell voltage will be redefined as the cell voltage at which the overall efficiency is reduced to 65%. In pressure-optimized operation, the current density of 2.67 A per cm^2 is achieved at a terminal cell voltage of 1.83 V for the system at 60 °C. The system at 90 °C achieves 3.20 A per cm^2 at a terminal cell voltage of 1.82 V.

(b) According to Fig. 1b, the overall efficiency difference of the system operating at 60 °C is 1.6% better than in the case of 90 °C at 3.20 A per cm^2. In comparison, the pressure optimization of the system turns it around (see Fig. 2b). The advantage of the system operating at 90 °C is 1.5%. It can be concluded that it strongly depends on the pressure mode if a hotter system is more efficient.

(c) In comparison to the results illustrated in Fig. 1b, the pressurized operation of the electrolyzer results in improved overall system efficiency. In particular, when the system operates at low current densities at 90 °C, its overall efficiency improves significantly by up to 5%. The best way to understand this increase is to compare Eq. (2) and the pressure curve in Fig. 2a. According to this equation, the hydrogen production efficiency increases with the electrode pressure, as the heat required for loading in the gas phase is reduced. However, the increase in pressure also increases the permeation of product gas across the membrane, thereby reducing the Faraday efficiency. Therefore, the pressure level needed to optimize the overall system's efficiency is always a compromise between reducing the external heat requirements and permeation. For a system operating at 90 °C, this increase in pressure is more significant than the water vapor pressure and the permeability coefficient increases.

For a better illustration of the last finding, Fig. 2b shows how the efficiency of hydrogen production, the Faraday efficiency and effort to compress the gas in external gas compressors contributes to the overall efficiency of the system operated at 90 °C (see also Eq. (4)). It is obvious that the overall efficiency of the system is predominated by the efficiency of hydrogen production, which is in accordance with previous studies. As mentioned before, this efficiency is limited by either the heat requirement or cell voltage. While eq. (2) describes the production efficiency of hydrogen in the case of heat limitation, the voltage limitation of production efficiency is described by Eq. (3). It can therefore be seen that at low current densities the hydrogen production efficiency is limited by heat requirements, while the voltage efficiency of the cell is up to 15% higher. Both efficiencies converge with increasing current densities, while at 2.21 A per cm^2, the difference is below 0.1% and equal at 2.38 A per cm^2. A difference of less than 0.1% in efficiency remains up to 2.57 A per cm^2. These findings can be compared with the optimal cathode pressure curve illustrated in Fig. 2a. The optimal cathode pressure increases until a local maximum of 2.15 MPa at 2.23 A per cm^2 is reached. With increasing current density, the optimal cathode pressure decreases to 0.94 MPa at 2.56 A per cm^2 and then starts rising in the direction of higher current densities again. In summary, there are two regions of increasing cathode pressure that are interrupted by a transition region between 2.23 and 2.56 A per cm^2. The center of the transition region at 2.39 A per cm^2 corresponds quite well to the contact point of the heat and voltage curves at 2.38 A per cm^2 (see Fig. 2b). Clearly, the first increase in the cathode pressure up to 2.23 A per cm^2 relates to the heat loss, while above 2.56 A per cm^2, the second region relates to the voltage efficiency. In the first region, an increase in the cathode pressure is attractive to reducing heat loss and compression work. However, higher values would increase Faraday losses too much. In the second region, the voltage efficiency limits the hydrogen production efficiency. Here, heat loss does not further affect the system efficiency, therefore making a further reduction by a pressure increase unnecessary. Consequently, the Faraday efficiency improves compared with the first region, while more compression work is also needed. In this region, the slope of the cathode pressure is lower than in the first region, which is mainly due to an equilibrium of the compression work and Faraday efficiency. It also means that, theoretically, the PEM-electrolyzer could operate at a higher temperature without causing additional heat loss, which would increase the hydrogen production efficiency, as the membrane conductivity and catalytic activity would increase. Clearly, the optimization process should aim to maximize the overall system efficiency by aligning the two cases of limiting hydrogen

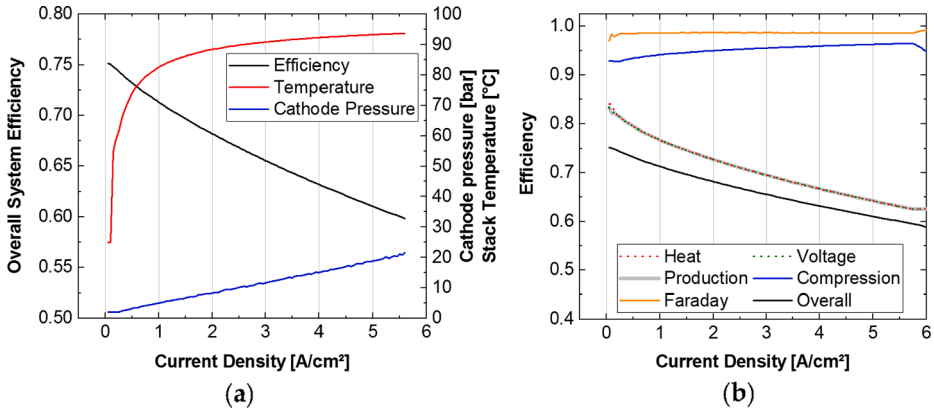

Fig. 3. (a) Plot of the overall system efficiency as a function of current density for a temperature- and pressure-optimized electrolyzer. This also illustrates the optimum cathode pressure and stack temperature as a function of current density; **(b)** plot of the efficiency contributions as a function of current density at optimized stack temperature. The curves for the heat, voltage and production are on top of each other.

production efficiency, namely heat loss and voltage efficiency. This finding is of great importance, as the heat and voltage efficiency of hydrogen production only match across a small current density range even if pressure optimization is applied. This suggests that the system does not work optimally within the rest of the current density range and that this cannot be achieved by pressure optimization alone, raising the question of what happens if the temperature can also be adjusted to optimize the overall system efficiency.

The result of this consideration is shown in Fig. 3a and 3b. If the electrolyzer is not only pressure-optimized, but also temperature-optimized, the thermal limitation of the hydrogen production efficiency is equal to the voltage efficiency across the entire current density range (see also Fig. 3b). In this case, a continuous increase appears in the cathode pressure curve and indicates that there are no longer two regions in which the electrolyzer is limited by either heat loss or voltage efficiency. In addition, the pressure at any operating point is lower than in the previous case, except at 2.38 A per cm^2. Here, the pressure is identical for both pressure-optimization at 90 °C and combined pressure and temperature optimization. This point specified the operating point at which the thermal and voltage efficiency are the same. Consequently, in the pressure–temperature-optimized case, the optimal temperature is precisely 90 °C. In principle, the combined optimization therefore determines the pressure level for each temperature where heat loss and overpotential are the same. This drastically contradicts the general assumption regarding increasing the efficiency of an electrolyzer by elevating the temperature as much as possible. It turns out that the optimal stack temperature increases with the current density. The assumption that electrolyzers must be developed in such a way that they can operate at temperatures above 90 °C is highly questionable due to the results displayed in Fig. 3a [10]. A temperature of 90 °C is only desirable for cell voltages above 1.76 V and 2.55 A per cm^2. Here, the overall system efficiency is decreased to 66.7%, which is only slightly above the defined goal of not operating below 65%. In addition, the cell voltage of 1.76 V precisely corresponds to the goal of achieving an efficiency of more than 70% before compression by 2030. Given that in addition to the lower efficiency, the durability of the system operated at 90 °C is also reduced, arguments for high temperatures do not hold up against the results reported here. The decrease in current density even causes the optimal stack temperature to approach room temperature as the thermoneutral cell voltage approaches 1.481 V. This is surprising, as the membrane conductivity and electrochemical activity is strongly decreased in this scenario.

An additional positive effect results from the reduced stack temperature with low current density. As the gas permeability through the membrane decreases at low temperatures, the Faraday efficiency increases, as can be seen in Fig. 3b. This means that less hydrogen permeates through the membrane, which is desirable as safety problems arise with volume fractions of hydrogen in oxygen higher than 4% because the mixture is explosive. Commonly used strategies to prevent high permeation rates are a thicker membrane, a lower cathode pressure or a recombination catalyst layer [37]. Fig. 4a shows the impact of the novel strategy. If the stack temperature and cathode pressure are kept constant at 90 °C and 1 MPa across the entire current density range, a Nafion 212 membrane-based system shows significant amounts of

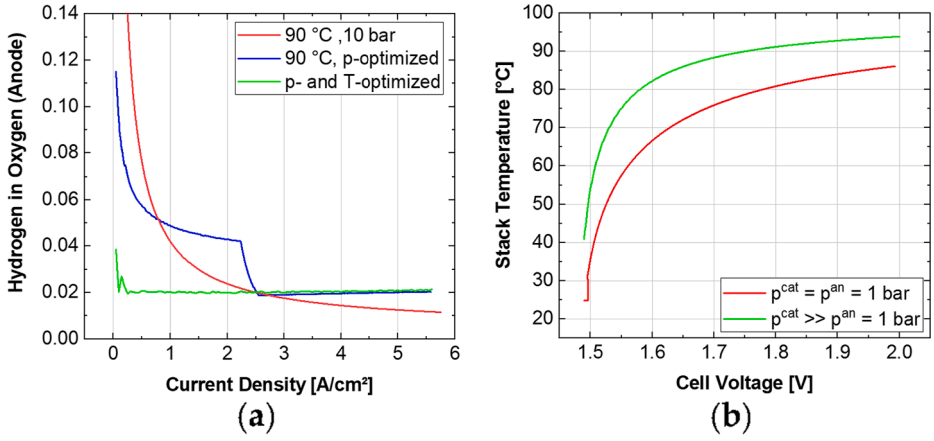

Fig. 4. (a) Plot of the volume fraction of hydrogen in oxygen at the cathode as a function of current density under different conditions; **(b)** plot of the ideal stack temperature (T greater than 25 °C) as a function of cell voltage.

hydrogen in oxygen at the anode at low and medium current densities. Therefore, the hydrogen crossover through the membrane must be reduced by either a thicker membrane or a recombination catalyst layer. While a steady drop in the hydrogen content in oxygen occurs for a constant pressure such as 1 MPa, the situation changes when the system is operated at optimal pressure. Here, the hydrogen content develops according to the corresponding pressure curve that is illustrated in Fig. 2a. In a first drop, the hydrogen content reaches a value of about 4% at 2.23 A per cm^2, which is precisely the position of the local cathode pressure maximum. This is followed by a sharp decrease in the hydrogen content of oxygen according to the transition zone up to 2.56 A per cm^2. During the second increase in the cathode pressure, the hydrogen content in oxygen remains almost the same, at about 2%. It is obvious that a pressure optimization does not lead to a sufficient defusing of the situation and thicker membranes or a recombination catalyst layer is still required. Combining the pressure optimization with the temperature optimization leads to a massive decrease in the hydrogen concentration in oxygen, especially at low current densities. In this case, the hydrogen content in oxygen is about 2% over the entire current density range, which is below the explosive limit of 4%. In the related simulation result, a non-monotonous course appears that is due to an applied minimum stack temperature of 25 °C. Accordingly, Fig. 3b also indicates a small deviation between the thermal and voltage efficiency at a very low current density due to this fact. However, this would disappear if the boundary condition was not given. In summary, this novel approach of combined temperature and pressure optimization is not a compromise between security requirements and performance, but rather reduces security challenges while simultaneously optimizing the system efficiency.

The question remains as to how the best temperature can be determined for a certain operating point without the need for computer-based simulations. Fortunately, an analytical solution for pressure-optimized systems is available, which is outlined below.

As can be seen in Fig. 3b, the voltage efficiency is equal to the heat-limited hydrogen production efficiency. Therefore, the denominator in Eq. (2) must be equal to the cell voltage, which is the denominator in Eq. (3). Consequently, the cell voltage becomes a function that depends exclusively on the partial pressures of oxygen at the anode and hydrogen at the cathode and on the water partial pressure in the electrodes. If it is assumed that the product gases in the electrode are saturated with vapor, the partial pressure of water can be substituted by any function that approximates the vapor pressure of water. These are often written in accordance with Eq. (5):[38]

$$p_{H_2O}^{sat} = A \cdot \exp\left(\frac{B \cdot T_{stack}}{C + T_{stack}}\right) \tag{5}$$

A, B and C are constants of the applied model, with the Magnus values being used for the simulations shown here (see Table S1).

Because the denominator in Eq. (2) contains the partial pressures, it must be modified slightly to include the total pressure in the electrodes. Accordingly, the optimal cell voltage as a function of the vapor pressure of water and electrode pressures is given by Eq. (6):

$$U_{cell} = U_{th} + \left[\frac{p_{H_2O}^{sat}}{p^{cat} - p_{H_2O}^{sat}} + \frac{p_{H_2O}^{sat}}{2 \cdot \left(p^{an} - p_{H_2O}^{sat}\right)}\right] \cdot \frac{\Delta H_{H_2O}^{vap}}{2\mathrm{F}} \tag{6}$$

The conversion of this equation to the solution of the optimal vapor pressure of water leads to the following equation:

$$p_{H_2O}^{sat,opt} = \frac{1}{2(\beta+3)} \cdot \left\{ p^{an}(\beta+2) + p^{cat}(\beta+1) - \sqrt{\left(-p^{an}(\beta+2) - p^{cat}(\beta+1)\right)^2 - 4p^{an}p^{cat}\beta(\beta+3)} \right\} \tag{7}$$

The new parameter, β, contains the cell voltage, thermoneutral cell voltage and the heat of vaporization. It is:

$$\beta = \frac{4\mathrm{F} \cdot (U_{cell} - U_{th})}{\Delta H_{H_2O}^{vap}} \tag{8}$$

In the following, it is assumed that the thermoneutral cell voltage and heat of vaporization are constants, which enables an analytical solution for the system. The impact of this assumption on the result is discussed below. The optimal stack temperature can be calculated by combining Eq. (5) and Eq. (7), which leads to the following equation:

$$T_{stack,opt} = \frac{C \cdot \ln\left(\frac{p_{H_2O}^{sat,opt}}{A}\right)}{B - \ln\left(\frac{p_{H_2O}^{sat,opt}}{A}\right)} \tag{9}$$

The expression of Eq. (7) simplifies for typical operating conditions of PEM-electrolyzers:

a) If the anode is at low pressure and the cathode is at high pressure, the first term in the brackets of Eq. (6) will become negligibly small. This high differential pressure mode simplifies Eq. (7) and is:

$$p_{H_2O}^{sat,opt} = \frac{\beta \cdot p^{an}}{\beta + 1} \tag{10}$$

b) If the mechanical stability of the membrane is low or the oxygen produced should also be stored, the balance pressure mode makes sense. With the pressures in the anode and cathode being the same, Eq. (7) leads to the following expression:

$$p_{H_2O}^{sat,opt} = \frac{\beta \cdot p^{an}}{\beta + 3} \tag{11}$$

The result of this consideration is shown graphically in Fig. 4b. The diagram shows the optimal temperature for systems with pressure optimization when operating with balance and in high differential pressure mode. Additionally, these curves determine the upper and lower limits for the optimal temperature for each pressure- and temperature-optimized system.

Eq. (5) to Eq. (11) describe the optimal temperature of a PEM-electrolyzer stack. This temperature is a function of the optimal water vapor pressure, which itself depends on the electrode pressures, cell voltage, thermoneutral cell voltage and the heat of vaporization. As is stated, the thermoneutral cell voltage and heat of vaporization are assumed to be constant. When calculating the optimal temperature, the resulting error from this assumption is less than 0.3 °C, between 60 °C and 90 °C, and about 0.9 °C at 25 °C. Accepting this error, no numerical solutions are required to calculate the optimal stack temperature. Surprisingly, only the electrode pressure and cell voltage remain as variables. Therefore, the optimal stack temperature of a PEM-water electrolyzer does not depend on its membrane material or thickness, its catalyst material or catalyst loading or further system parameters. These findings have a fundamental impact on how PEM-water electrolyzers should be operated in order to obtain the best performance. To the best of our knowledge, it is a general solution for this technology. However, the boundary conditions must be met and technical challenges are clear:

a) The model is imprecise when the membrane is very thin (less than20 μm) and room temperature is assumed as the lower temperature limit. In this case, hydrogen permeation across the membrane is dominant and cannot be eliminated by temperature adjustment.
b) The heat loss in the rest of the system must be negligible compared with that due to loading in the gas phase. This condition is more likely to be met by large- than laboratory-scale systems, because the thermal mass is much higher compared to the heat loss by surfaces.
c) PEM-electrolyzers are favorable in hydrogen production from renewables due to their fast response to load changes, but PEM-electrolyzers are not limited to dynamic operation. Technically, a fast adjustment of the stack temperature is critical to achieve, as the thermal mass is high. However, novel technical solutions could narrow this gap in future.
d) While the presented model is an analysis of the static case, future work should focus on how to maximize the efficiency by pressure and temperature changes during dynamic operation.

4. Conclusions

The starting point of this discussion was that the performance of polymer electrolyte membrane water-electrolyzers would improve with increasing operating temperatures, which has a negative impact on the durability of the systems due to accelerated corrosion processes. This study therefore examined the influence of temperature on the overall system efficiency with some surprising results that contradict the previous understanding of the operating conditions of polymer electrolyte membrane water-electrolyzers. While there is no doubt about the fact that a polarization curve improves with increasing stack temperature, some stunning effects were shown in the overall performance of the system. It was demonstrated that research and development do not need to focus on the development of durable materials for operation at 90 °C, as the optimal stack temperature is lower within the relevant current density range, which is limited by efficiency requirements. In contrast, the optimal temperature approaches ambient at low current densities and increases with the current density, reaching a value of 80 °C at about 1.6 V. While this optimizes the overall system efficiency, the safety problem that arises from hydrogen permeation across the membrane, resulting in the generation of explosive gases on the oxygen side, is also diminished due to a slower permeation process. In addition to these two factors, there is a third advantage in that the lower stack temperature also increases stack durability. Ultimately, it has been shown that the optimal temperature cannot only be determined by computer-based simulations, but its course also results from an analytically-solvable function.

CRediT authorship contribution statement

Fabian Scheepers: Conceptualization, Methodology, Software, Validation, Formal analysis, Investigation, Resources, Data curation, Writing - original draft, Writing - review & editing, Visualization. **Markus Stähler:** . **Andrea Stähler:** . **Edward Rauls:** . **Martin Müller:** Supervision. **Marcelo Carmo:** Supervision. **Werner Lehnert:** Supervision, Project administration.

Declaration of Competing Interest

The authors declared that there is no conflict of interest.

Appendix A

This section provides an overview of the model. Detailed information on the model, the selection of parameters and other assumptions have been previously published [31].

Nomenclature (Appendix)

Parameter	Symbol
Magnus parameter	A
Water activity (membrane)	$a^m_{H_2O}$
Current effect on permeation	a_x
Magnus parameter	B
Magnus parameter	C
Compression factor	c_c
Membrane thickness	d^m
Energy	E
Activation energy (anode)	E_A
Activation energy (membrane)	E_m
Faraday constant	F
Gibbs free energy	G
Enthalpy	H
Higher heating value	HHV
Current density	j
Exchange current density	j_0
Lower heating value	LHV
Amount of substance	n
Permeability	P
Pressure	p
Storage pressure	p^s
Gas constant	R
Reference value	Ref
Contact resistance	R_0
Entropy	S
Number of compressor stages	s_c
Temperature	T
Activation overpotential	U_{act}
Cell voltage	U_{cell}

(*continued on next page*)

(*continued*)

Parameter	Symbol
Voltage equivalency (LHV)	U_{LHV}
Voltage equivalency (vapor load)	U_{load}
Nernst voltage	U_N
Ohmic overpotential	U_{res}
Reversible cell voltage	U^0_{rev}
Thermoneutral cell voltage	U_{th}
Total compression work	W_c
Compression work per stage	W^1_c
Compressibility factor	Z
Number of transferred electrons	z
Charge transfer coefficient	α
Heat of vaporization	$\Delta H^{vap}_{H_2O}$
Membrane swelling factor	δ^m
Efficiency of gas compressor	η_c
Effort for external gas compression	$\eta^c_{H_2}$
Faraday efficiency	$\eta^F_{H_2}$
(Hydrogen) production efficiency	η^p
Overall system efficiency	$\eta^{tot}_{H_2}$
Heat capacity factor	κ
Ionic conductivity (membrane)	σ^m

(A) Hydrogen production efficiency

Hydrogen production efficiency, including the loading of the gas phase, can be written as:

$$\eta^p_{H_2} = \frac{E_{out}}{E_{in}} = \frac{n_{H_2}\Delta H_{LHV}}{\underbrace{\underbrace{n_{H_2}\Delta G_{LHV}}_{electric} + \underbrace{n_{H_2}T\Delta S}_{heat}}_{=n_{H_2}\Delta H_{LHV}} + \underbrace{n_{H_2}(\Delta H_{HHV} - \Delta H_{LHV})}_{vaporization} + \underbrace{n_{H_2O}\Delta H_{vap}}_{loading}} \tag{S1}$$

The water required for saturating the gas-phase produced in the electrolyzer is the sum of the water that evaporates at the anode and cathode. When an ideal gas and Dalton's law are assumed, it is:

$$n_{H_2O} = n^{cat}_{H_2O} + n^{an}_{H_2O} \tag{S2}$$

$$n^{cat}_{H_2O} = \frac{p^{cat}_{H_2O}}{p^{cat}_{H_2}} n_{H_2} \tag{S3}$$

$$n^{an}_{H_2O} = \frac{p^{an}_{H_2O}}{p^{an}_{O_2}} n_{O_2} \tag{S4}$$

It is $p^{cat}_{H_2O} = p^{an}_{H_2O}$ because both electrodes are at the same temperature:

$$n_{H_2O} = p^{cat}_{H_2O}\left(\frac{1}{p^{cat}_{H_2}} n_{H_2} + \frac{1}{p^{an}_{O_2}} n_{O_2}\right) \tag{S5}$$

During electrolysis, twice the amount of hydrogen is produced compared to oxygen ($n_{O_2} = \frac{1}{2} n_{H_2}$):

$$n_{H_2O} = n_{H_2} p^{cat}_{H_2O}\left(\frac{1}{p^{cat}_{H_2}} + \frac{1}{2p^{an}_{O_2}}\right) \tag{S6}$$

Inserting into Eq. (S1) results in:

$$\eta^p_{H_2} = \frac{\Delta H_{LHV}}{\Delta H_{HHV} + p^{cat}_{H_2O}\left(\frac{1}{p^{cat}_{H_2}} + \frac{1}{2p^{an}_{O_2}}\right)\Delta H_{vap}} \tag{S7}$$

Dividing the enthalpy by 2F, this is equal to eq. 2.

(B) Cell voltage modeling

The cell voltage is the sum of the Nernst voltage, U_{cell}, the activation overpotential, U_{act}, and the electric resistance, U_{res}, of the cell. For electrolysis, the mass transfer resistance overpotential can be neglected, and is:

$$U_{cell} = U_N + U_{act} + U_{\text{res}} \tag{S8}$$

The Nernst voltage, which includes the partial pressures at the electrodes, is:

$$U_N = E^{an} - E^{cat} = U^0_{rev} + \frac{\mathrm{R}T_{stack}}{2\mathrm{F}} \ln\left(\sqrt{\frac{p^{an}_{O_2}}{p_0}}\ \frac{p^{cat}_{H_2}}{p_0}\right) \tag{S9}$$

This equation includes the reversible cell voltage: [39]

$$U^0_{rev} = 1.229\mathrm{V} - 0.9 \cdot 10^{-3} \cdot (T_{stack} - 298\mathrm{K})\frac{\mathrm{V}}{\mathrm{K}} \tag{S10}$$

Table S1
These parameter values were used for the simulations.

Symbol	Value	Unit	Ref.
A	610.94	Pa	[38]
B	17.625	-	[38]
C	234.04	°C	[38]
ΔH_{vap}	41,572	J mol^{-1}	
$P_{H_2}^{80^\circ C}$	$5.31 \cdot 10^{-16}$	mol (cm s Pa)$^{-1}$	[24]
σ^m	0.137	S cm^{-1}	[42]
d^m	$51 \cdot 10^{-4}$	cm	
δ^m	1.15	-	[43]
c_c	2.75	-	[26]
T_{in}	300	K	
κ	1.4	-	
η_c	0.825	-	[44]
$p_{H_2}^s$	20	MPa	[45]
α	0.43	-	[31]
j_0	$8 \cdot 10^{-6}$	A cm^{-2}	[31]
a_x	$1.2 \cdot 10^{-5}$	cm	[31]
R_0	27	mOhm cm^2	[31]
E_A	40000	J mol^{-1}	[46]
E_m	20000	J mol^{-1}	[40]
T_{ref}	353.15	K	
p_{ref}	101325	Pa	
$a_{H_2O}^m$	1	-	

For the activation overpotential, the Tafel equation can be used as an approximation. It can be assumed that the cathode activation overpotential is small compared to the anode activation overpotential:

$$U_{act} = \frac{RT_{stack}}{\alpha z F} \ln\left(\frac{j}{j_0}\right) \tag{S11}$$

The anode exchange current density, j_0, is a function of the activation energy, E_A, and the stack temperature. It is:

$$j_0 = j_{0,ref} \cdot \exp\left[-\frac{E_A}{RT_{stack}}\left(1 - \frac{T_{stack}}{T_{ref}}\right)\right] \tag{S12}$$

The electric resistance of the cell is calculated according to Ohm's law. It depends on the interface resistance, R_0, the thickness, d^m, and the swelling, δ^m, of the membrane and the membrane resistance, σ^m:

$$U_{res} = \left(R_0 + \frac{d^m \delta^m}{\sigma^m\left(T_{cell}; a_{H_2O}^m\right)}\right) \cdot j \tag{S13}$$

The ionic conductivity of Nafion membranes were experimentally validated to be a function of the water activity, $a_{H_2O}^m$, in the membrane:[40]

$$\sigma^m = \left(0.6877 + a_{H_2O}^m\right)^3 \exp\left(-\frac{10440 \cdot a_{H_2O}^{m\,\frac{1}{4}}}{RT_{stack}}\right) \tag{S14}$$

(C) Faraday efficiency

The Faraday efficiency is calculated with:

$$\eta_{H_2}^F = \frac{E_{out}}{E_{in}} = \frac{\left(n_{H_2}^p - n_x\right)\Delta H_{LHV}}{n_{H_2}^p \Delta H_{LHV}} = \frac{j - j_x}{j} = 1 - \frac{j_x}{j} \tag{S15}$$

The crossover current density of hydrogen through the membrane is: [40]

$$j_{x,H_2} = 2\left(F \cdot P_{H_2}^T \cdot \frac{p_{H_2}^{cat}}{d^m \delta^m} + \frac{a_x}{d^m \delta^m} j\right) \exp\left[\frac{E_m}{R}\left(\frac{1}{T_{ref}} - \frac{1}{T_{stack}}\right)\right] \tag{S16}$$

here, $P_{H_2}^T$ is the permeability coefficient and a_x expresses the increase in permeation with increasing current density. The permeation coefficient is temperature-dependent, with E_m as the activation energy for this process. The total gas crossover current density, j_x, is the sum of the permeation current density of oxygen and hydrogen. While only half of the oxygen is produced compared with hydrogen, the permeability coefficient was also measured to be only half the size [24]. Assuming the same increase in permeation as a function of current density, this yields:

$$j_x \approx 2\left[F \cdot P_{H_2}^T \cdot \frac{p_{H_2}^{cat} + p_{O_2}^{an}}{d^m \delta^m} + \frac{2a_x}{d^m \delta^m} j\right] \exp\left[\frac{E_m}{R}\left(\frac{1}{T_{ref}} - \frac{1}{T_{stack}}\right)\right] \tag{S17}$$

(D) Effort for gas compression

The effort expresses the ratio of work that is required to compress the gas, W_c, and the hydrogen that can be stored by taking into account the mechanical efficiency of the gas compressors, η_c: [31]

$$\eta_{H_2}^{c} = 1 - \frac{W_c}{(n_{H_2} - n_x)\Delta H_{LHV}} \cdot \frac{1}{\eta_c} \tag{S18}$$

The total compression work is the sum of the compression work of each stage. It is assumed that the compression factor per stage is the same. Therefore, the total compression work is the product of the compression work per stage and the number of stages:

$$W_c = s_c \cdot W_c^1 \tag{S19}$$

Each stage requires a compression work that depends on the compression factor, c_c, the initial gas temperature before the compression, T_{in}, and the heat capacity ratio, κ: [41]

$$W_c^1 = \frac{\kappa}{\kappa - 1}(n_{H_2} - n_x)\mathrm{R}T_{in}Z\left(c_c^{\frac{\kappa-1}{\kappa}} - 1\right) \tag{S20}$$

The number of compressor stages to achieve the storage pressure, $p_{H_2}^s$, is determined by:

$$s_c = \frac{\log\left(\frac{p_{H_2}^s}{p^{cat}}\right)}{\log(c_c)} \tag{S21}$$

(E) Parameter values

For our simulations, we used the parameters listed in Table S1.

References

[1] Kuntke P, Rodríguez Arredondo M, Widyakristi L, ter Heijne A, Sleutels THJA, Hamelers HVM, et al. Hydrogen Gas Recycling for Energy Efficient Ammonia Recovery in Electrochemical Systems. Environ Sci Technol 2017;51(5):3110–6.

[2] Muradov N. Low to near-zero CO2 production of hydrogen from fossil fuels: Status and perspectives. Int J Hydrogen Energy 2017;42(20):14058–88.

[3] The Future of Hydrogen - Seizing today's opportunities; International Energy Agency: 2019; p 203.

[4] Hank C, Gelpke S, Schnabl A, White RJ, Full J, Wiebe N, et al. Economics & carbon dioxide avoidance cost of methanol production based on renewable hydrogen and recycled carbon dioxide – power-to-methanol. Sustainable Energy Fuels 2018;2(6):1244–61.

[5] Global Warming of 1.5 °C - Summary for Policymakers; Intergovernmental Panel on Climate Change: 2018; p 32.

[6] Gür TM. Review of electrical energy storage technologies, materials and systems: challenges and prospects for large-scale grid storage. Energy Environ Sci 2018;11(10):2696–767.

[7] Kayfeci M, Keçebaş A, Bayat M. Chapter 3 - Hydrogen production. In: Calise F, D'Accadia MD, Santarelli M, Lanzini A, Ferrero D, editors. Solar Hydrogen Production. Academic Press; 2019. p. 45–83.

[8] Shaner MR, Atwater HA, Lewis NS, McFarland EW. A comparative technoeconomic analysis of renewable hydrogen production using solar energy. Energy Environ Sci 2016;9(7):2354–71.

[9] Schmidt O, Gambhir A, Staffell I, Hawkes A, Nelson J, Few S. Future cost and performance of water electrolysis: An expert elicitation study. Int J Hydrogen Energy 2017;42(52):30470–92.

[10] Babic U, Suermann M, Büchi FN, Gubler L, Schmidt TJ. Critical Review—Identifying Critical Gaps for Polymer Electrolyte Water Electrolysis Development. J Electrochem Soc 2017;164(4):F387–99.

[11] Ayers KE, Anderson EB, Capuano C, Carter B, Dalton L, Hanlon G, et al. Research Advances towards Low Cost, High Efficiency PEM Electrolysis. ECS Trans 2010;33(1):3–15.

[12] Chandesris M, Médeau V, Guillet N, Chelghoum S, Thoby D, Fouda-Onana F. Membrane degradation in PEM water electrolyzer: Numerical modeling and experimental evidence of the influence of temperature and current density. Int J Hydrogen Energy 2015;40(3):1353–66.

[13] Fouda-Onana F, Chandesris M, Médeau V, Chelghoum S, Thoby D, Guillet N. Investigation on the degradation of MEAs for PEM water electrolysers part I: Effects of testing conditions on MEA performances and membrane properties. Int J Hydrogen Energy 2016;41(38):16627–36.

[14] Frensch SH, Fouda-Onana F, Serre G, Thoby D, Araya SS, Kær SK. Influence of the operation mode on PEM water electrolysis degradation. Int J Hydrogen Energy 2019;44(57):29889–98.

[15] Millet P, Ngameni R, Grigoriev SA, Mbemba N, Brisset F, Ranjbari A, et al. PEM water electrolyzers: From electrocatalysis to stack development. Int J Hydrogen Energy 2010;35(10):5043–52.

[16] Yigit T, Selamet OF. Mathematical modeling and dynamic Simulink simulation of high-pressure PEM electrolyzer system. Int J Hydrogen Energy 2016;41(32):13901–14.

[17] Selamet ÖF, Acar MC, Mat MD, Kaplan Y. Effects of operating parameters on the performance of a high-pressure proton exchange membrane electrolyzer. Int J Energy Res 2013;37(5):457–67.

[18] Awasthi A, Scott K, Basu S. Dynamic modeling and simulation of a proton exchange membrane electrolyzer for hydrogen production. Int J Hydrogen Energy 2011;36(22):14779–86.

[19] Toghyani S, Afshari E, Baniasadi E, Atyabi SA, Naterer GF. Thermal and electrochemical performance assessment of a high temperature PEM electrolyzer. Energy 2018;152:237–46.

[20] Lee B, Park K, Kim HM. Dynamic Simulation of PEM Water Electrolysis and Comparison with Experiments. Int J Electrochem Sci 2013;8:235–48.

[21] Tugirumubano A, Kwac L, Lee M, Lee J, Lee J, Jeon S, et al. Analysis of the Parametric Effect on the Performance of a Polymer Electrolyte Membrane Electrolyzer. International Journal of Mechanical Engineering and Robotics Research 2017;6:1–5.

[22] Zhang H, Su S, Lin G, Chen J. Efficiency Calculation and Configuration Design of a PEM Electrolyzer System for Hydrogen Production. Int J Electrochem Sci 2012;7.

[23] Schalenbach M, Carmo M, Fritz DL, Mergel J, Stolten D. Pressurized PEM water electrolysis: Efficiency and gas crossover. Int J Hydrogen Energy 2013;38(35):14921–33.

[24] Schalenbach M. Corrigendum to "Pressurized PEM water electrolysis: Efficiency and gas crossover" [Int J Hydrogen Energy 38 (2013) 14921–14933]. Int J Hydrogen Energy 2016;41(1):729–32.

[25] Tjarks G, Gibelhaus A, Lanzerath F, Müller M, Bardow A, Stolten D. Energetically-optimal PEM electrolyzer pressure in power-to-gas plants. Appl Energy 2018;218:192–8.

[26] Bensmann B, Hanke-Rauschenbach R, Peña Arias IK, Sundmacher K. Energetic evaluation of high pressure PEM electrolyzer systems for intermediate storage of renewable energies. Electrochim Acta 2013;110:570–80.

[27] Suermann M, Kiupel T, Schmidt TJ, Buchi FN. Electrochemical Hydrogen Compression: Efficient Pressurization Concept Derived from an Energetic Evaluation. J Electrochem Soc 2017;164(12):F1187–95.

[28] Sartory M, Wallnöfer-Ogris E, Salman P, Fellinger T, Justl M, Trattner A, et al. Theoretical and experimental analysis of an asymmetric high pressure PEM water electrolyser up to 155 bar. Int J Hydrogen Energy 2017;42(52):30493–508.

[29] Santarelli M, Medina P, Calì M. Fitting regression model and experimental validation for a high-pressure PEM electrolyzer. Int J Hydrogen Energy 2009;34(6):2519–30.

[30] García-Valverde R, Espinosa N, Urbina A. Simple PEM water electrolyser model and experimental validation. Int J Hydrogen Energy 2012;37(2):1927–38.

[31] Scheepers F, Stabler M, Stabler A, Rauls E, Muller M, Carmo M, et al. Improving the Efficiency of PEM Electrolyzers through Membrane-Specific Pressure Optimization. Energies 2020;13(3).

[32] Carmo M, Fritz DL, Mergel J, Stolten D. A comprehensive review on PEM water electrolysis. Int J Hydrogen Energy 2013;38(12):4901–34.

[33] Path to hydrogen competitiveness - A cost perspective; Hydrogen Council: 2020; p 88.

[34] 34. Bertuccioli, L.; Chan, A.; Hart, D.; Lehner, F.; Madden, B.; Standen, E. Study on development of water electrolysis in the EU; e4tech: Lausanne, 2014.

[35] Mayyas, A. T.; Ruth, M. F.; Pivovar, B. S.; Bender, G.; Wipke, K. B. Manufacturing Cost Analysis for Proton Exchange Membrane Water Electrolyzers; NREL/TP-6A20-72740 United States 10.2172/1557965 NREL English; ; National Renewable Energy Lab. (NREL), Golden, CO (United States): 2019; p Medium: ED; Size: 3.3 MB.

[36] Trinke P, Bensmann B, Hanke-Rauschenbach R. Current density effect on hydrogen permeation in PEM water electrolyzers. Int J Hydrogen Energy 2017;42(21):14355–66.

[37] Klose C. Membrane Interlayer with Pt Recombination Particles for Reduction of the Anodic Hydrogen Content in PEM Water Electrolysis. J Electrochem Soc 2018;165(16):F1271–6.

[38] Alduchov OA, Eskridge RE. Improved Magnus Form Approximation of Saturation Vapor Pressure. J Appl Meteorol 1996;35(4):601–9.

[39] Harrison KW, Hernández-Pacheco E, Mann M, Salehfar H. Semiempirical Model for Determining PEM Electrolyzer Stack Characteristics. J Electrochem Energy Convers Storage 2005;3(2):220–3.

[40] Trinke P, Bensmann B, Reichstein S, Hanke-Rauschenbach R, Sundmacher K. Hydrogen Permeation in PEM Electrolyzer Cells Operated at Asymmetric Pressure Conditions. J Electrochem Soc 2016;163(11):F3164–70.
[41] Tzimas, E.; Filiou, C.; Peteves, S.; Veyret, J., Hydrogen storage: state-of-the-art and future perspective. EU Commission, JRC Petten, EUR 20995EN 2003.
[42] Yadav R. Analysis of EIS Technique and Nafion 117 Conductivity as a Function of Temperature and Relative Humidity. J Electrochem Soc 2012;159(3):B340–6.
[43] Shi S, Weber AZ, Kusoglu A. Structure/property relationship of Nafion XL composite membranes. J Membr Sci 2016;516:123–34.
[44] Dehnen, M. Hofer Diaphragm Compressors; Hofer Hochdrucktechnik GmbH.
[45] Witkowski A, Rusin A, Majkut M, Stolecka K. Comprehensive analysis of hydrogen compression and pipeline transportation from thermodynamics and safety aspects. Energy 2017;141:2508–18.
[46] Lettenmeier P, Wang L, Golla-Schindler U, Gazdzicki P, Cañas NA, Handl M, et al. Nanosized IrOx–Ir Catalyst with Relevant Activity for Anodes of Proton Exchange Membrane Electrolysis Produced by a Cost-Effective Procedure. Angew Chem Int Ed 2016;55(2):742–6.